FFI Norwegian Defence Research Establishment

22/01519

FFI-RAPPORT

Automatic Underway AUV Recovery Using a USV

Glenn Bitar
Marius Rundhovde
Else-Line Malene Ruud
Jarle Sandrib
Jarle Selvåg
Ragnar Smestad

Automatic Underway AUV Recovery Using a USV

Glenn Bitar
Marius Rundhovde
Else-Line Malene Ruud
Jarle Sandrib
Jarle Selvåg
Ragnar Smestad

Norwegian Defence Research Establishment (FFI) 12 September 2022

Keywords
Autonome undervannsfartøyer (AUV)
Autonomi
Styring og kontroll
Ubemannede overflatefartøyer (USV)

FFI report
22/01519

Project number
1636, 1505

Electronic ISBN
978-82-464-3419-3

Approvers
Håkon Storli Andersen, *Director of Research*
Rikke Amilde Seehuus, *Research Manager*
Morten Nakjem, *Research Manager*

The document is electronically approved and therefore has no handwritten signature.

(U) Summary

The future Norwegian naval mine countermeasure (NMCM) capability includes unmanned, autonomous vessels. The Royal Norwegian Navy uses the *Hugin* autonomous underwater vehicle (AUV) in mine hunting operations. To facilitate transportation and extension of *Hugin*'s operational range in NMCM operations, the Norwegian Defence Research Establishment (FFI) is developing technology for automatic launch and recovery of AUVs using unmanned surface vehicles (USVs). This report describes the *Stinger* launch and recovery system (LARS) mounted onto the USV *Frigg*, a method for automatic recovery of the *Hugin* AUV using this system, and a system that can estimate relative position and velocity of the AUV using a lidar sensor mounted on the USV. Results from full-scale experiments are also presented.

(U) Sammendrag

Sjøforsvaret vil i stor grad benytte ubemanna, autonome farkoster i sine framtidige kapabiliteter for mottiltak mot miner. For eksempel benyttes den autonome undervannsdrona (AUV-en) *Hugin* for minejaktoperasjoner. Det er viktig å legge til rette for transport av *Hugin*, og for å utvide dens operasjonelle rekkevidde. Derfor utvikler Forsvarets forskningsinstitutt (FFI) teknologi for automatisk utsetting og innhenting av AUV-er. Det kan gjøres ved hjelp av ubemanna overflatefartøy (USV-er). Denne rapporten beskriver utsettings- og innhentingssystemet (LARS) *Stinger*. Systemet er montert på USV-en *Frigg*. Rapporten beskriver en metode for automatisk innhenting av *Hugin* ved hjelp av dette systemet. Vi beskriver også et system som kan estimere den relative posisjonen og farta til AUV-en. Det gjøres ved hjelp av en lidarsensor som er montert på USV-en. Resultater fra fullskalaeksperimenter presenteres også.

Contents

Acronyms

AUV autonomous underwater vehicle

FFI Norwegian Defence Research Establishment
FRD forward-right-down

GNSS global navigation satellite system
GUI Graphical User Interface

HAL Hybrid Autonomy Layer

ILOS integral line of sight
INS inertial navigation system

LARS launch and recovery system

NED north-east-down
NMCM naval mine countermeasures

PD proportional-derivative
PLC programmable logic controller

ROS Robot Operating System

SA situational awareness
SAS synthetic aperture sonar

UHF ultra high frequency
USV unmanned surface vehicle

1 Introduction

The conceptual solution for the Royal Norwegian Navy's future naval mine countermeasures (NMCM) capability describes extensive use of modular autonomous systems. Moving the manned vessels outside of the mine danger area will reduce the personnel risk as they no longer need to work inside a mine danger area. The use of autonomous systems also reduces procurement cost, as the larger, crewed ships will not require full shock and signature specifications.

The future concept describes unmanned surface vehicles (USVs) supporting autonomous underwater vehicle (AUV) operations with logistics such as launching and recovering, and establishing a connection link between a submerged AUV and manned vessels. The operational uncertainty of where mines are located means that the USVs must be able to operate with standoff distances from manned ships where high-bandwidth communication is not always possible. Therefore, high-level of autonomous functionality specialized for AUV support operations is required on the USVs. Especially, the recovery of an AUV is a challenging task to perform without, or with minimal human intervention.

To address the technological uncertainty on the AUV recovery aspect, the Norwegian Defence Research Establishment (FFI) has, through dedicated research programs for NMCM, been developing technology demonstrators for USVs and a lightweight AUV launch and recovery system (LARS). This development has been supported by FFI's strategic investments in autonomy research, which includes building scalable frameworks for autonomy and situational awareness. Crucial autonomous behaviors have been implemented on FFI's USVs, such as the ability to transition between locations and perceive the surrounding environment. The technology demonstrator for AUV launch and recovery has also been taken to an operational experimental level where the concept can be tested on one of FFI's USVs and a modified *Hugin* class AUV.

This report describes the development and implementation of a method for performing recovery of the *Hugin* AUV while the AUV is underway. Results from full-scale experiments are also presented.

1.1 Background and motivation

NMCM includes detecting, locating, classifying, and neutralizing naval mines. There are several ways of performing NMCM-operations, including minesweeping and mine hunting. Minesweeping is the practice of a light ship or aircraft towing a magnetic field-inducing cable, or other equipment that simulates a heavier ship by producing environmental effects. The practice aims to neutralizing mines by provoking a detonation behind the towing vehicle.

Mine hunting is the process of detecting, locating, and classifying naval mines using sensors such as sonars and optical cameras, or mine diver personnel. The Navy have since 2004 been using the *Hugin* class AUV for this purpose, which autonomously detects and localizes mines using a synthetic aperture sonar (SAS). Read more about *Hugin* in (Hagen et al., 2009; Jalving, Kristensen and Størkersen, 1998).

Hugin operates on battery and has an operational speed of up to 4 kn. The stand-off distance required in the new concept, meant to keep manned vessels out of hazard, will therefore reduce the effective operational time of the AUV. To increase *Hugin*'s range of operation, and thereby restore the effective operational time, it is necessary to be able to transport it in and out of an operational area using USVs. To reduce the technological risk of this operation, FFI is developing technology for an USV that allows automatic recovery of *Hugin* after ended mission.

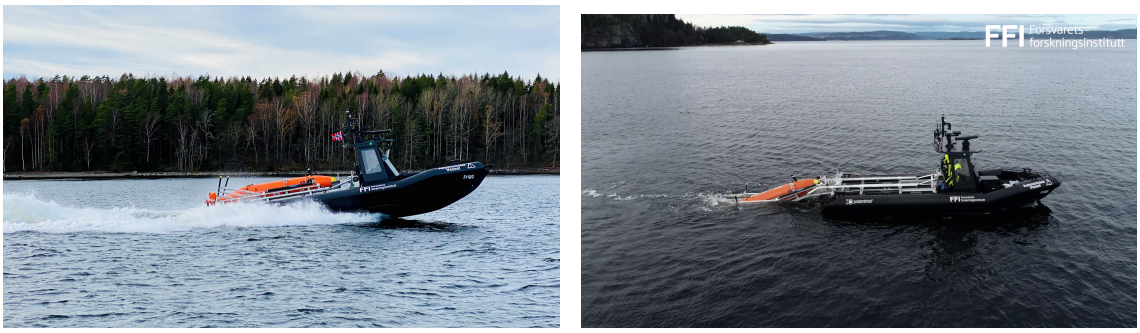

(a) Transportation. *(b) Launch.*

Figure 1.1 Pictures of the USV Frigg *with the* Stinger *LARS and the* Hugin *AUV.*

Hugin performs its tasks autonomously, but was designed to be launched and recovered manually from crewed vessels. The established procedure for manual recovery is to have the AUV dead in the water nearby a manned vessel, and to release *Hugin*'s nose cone which is attached to a recovery rope. The nose cone with this rope is then manually recovered by the ship's crew and attached to a LARS system. To adapt this procedure for unmanned recovery, the releasable nose cone was replaced by a hook, which together with a revised LARS system with an arresting line, make up the recovery system. When the arresting line and the nose hook make physical contact, *Hugin* is attached to the LARS and can be pulled on board. Pictures of the AUV-LARS system on-board the USV *Frigg* are displayed in Figure 1.1.

This new LARS configuration is designed for recovery in scenarios where the AUV is underway, and where it is dead in the water. For an autonomous recovery operation to be feasible in either scenario, the AUV must have power to relay its position and orientation to the recovering USV. The autonomous functionality required for both scenarios has several components in common, such as

- receiving telemetry from *Hugin*,
- fusing this telemetry with information from onboard sensors on the USV, such as lidar data, to more accurately estimate relative position and orientation, and
- safely navigating the USV in the vicinity of *Hugin* while minimizing collision risk.

In the early stages of developing autonomous functionality for AUV recovery for the USVs, we decided to start by solving the *underway* recovery scenario. This decision was mainly due to the belief that navigating the USV relative to *Hugin* would be easier with some steering speed, and development of this type of control method would take the shortest amount of time. Lessons from this development and testing would then be used to prepare and develop methods for the second scenario, where *Hugin* would lie dead in the water.

1.2 The *Frigg* USV and the HAL autonomy framework

FFI owns and operates two USVs of the *Odin* class, *Odin* and *Frigg*. They have furbished them with sensors and systems that give them autonomous capabilities. A description of its capabilities and software systems is available in (Ruud et al., 2020). The *Stinger* LARS, developed by *H. Henriksen*,[1] is mounted onto *Frigg*, and can be lowered behind the stern to launch and recover

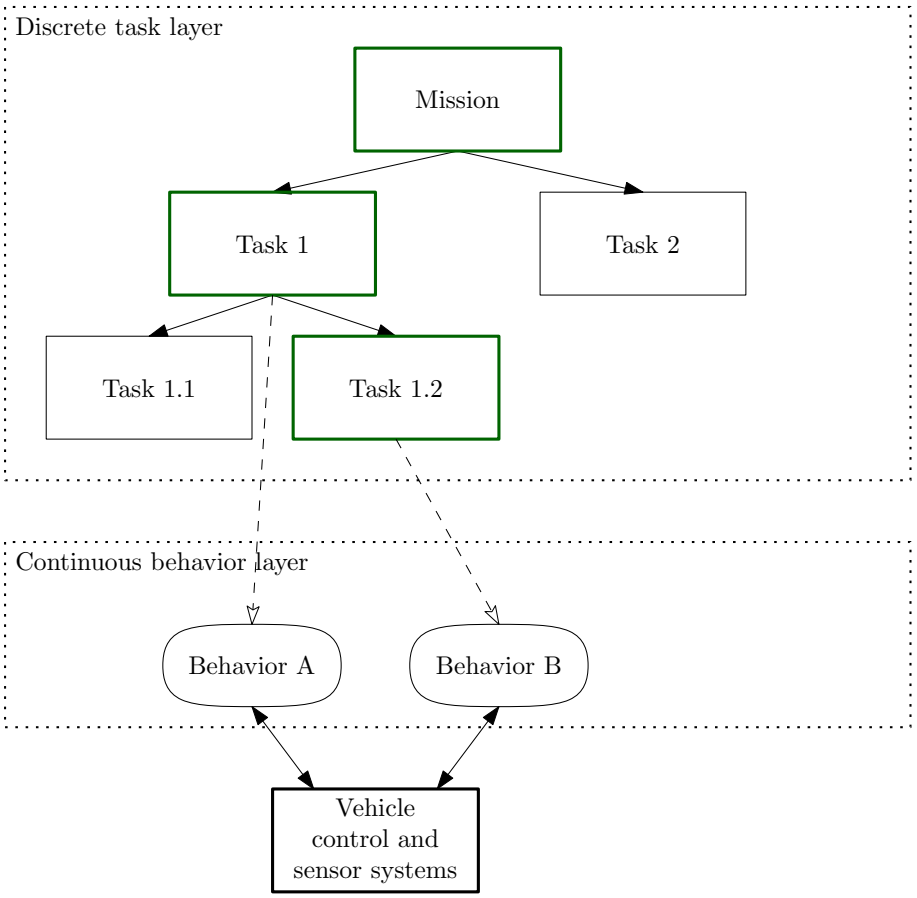

Figure 1.2 Conceptual overview of the decision autonomy framework HAL. The highlighted tasks represent the path of active tasks, that decide which behaviors are running in the behavioral layer.

Hugin, seen in Figure 1.1.

To implement autonomous functionality, *Frigg* runs the decision autonomy framework Hybrid Autonomy Layer (HAL). HAL comprises two control layers, which is a task tree and a behavioral layer, illustrated in Figure 1.2. The task tree represents discrete tasks, e.g., *move*, *turn*, and is hierarchical. One path from the top-level mission to a leaf task is *active* at a time. The active tasks decide which behaviors are present in the behavioral layer. The behavioral layer represents continuous control, such as a feedback loop controlling velocity, and the active behaviors interfaces with the vessel's control and sensor systems. More details on how HAL works are available in (Krogstad et al., 2020).

1.3 Relevant work

A comparable undertaking to the AUV recovery task described in this report, is presented in (Zarayskaya et al., 2019). That paper describes a contribution to the Shell Ocean Discovery

[1]Product site for a different version of the *Stinger* LARS:
`https://hhenriksen.com/launch-and-recovery-auv-stinger/` (accessed February 2, 2022).

XPRIZE competition,[2] where the overall goal was to autonomously map the ocean floor. The cited contribution used the USV *SEA-KIT* and the AUV *Hugin* for ocean floor mapping. The recovery procedure was a multi-step approach that started by having *SEA-KIT* follow *Hugin* while *Hugin* was submerged and following a waypoint line. They used the following-algorithm presented in (Simonsen and Ruud, 2020), where FFI contributed to its implementation on *SEA-KIT*. Subsequently, *SEA-KIT* was ordered to follow the same waypoint line while *Hugin* emerged to the surface. *SEA-KIT*'s speed was adjusted to reduce longitudinal distance, and lateral offset was corrected by manually commanding *Hugin* to apply an offset to its waypoint line. *SEA-KIT*'s hull is designed with a bespoke bed that is well-suited for recovering and storing *Hugin*, in contrast to *Frigg*, which is a multi-role USV, carrying the *Stinger* LARS for the same purpose.

A different method for launch and recovery of an AUV from a mother ship is presented in (Szczotka, 2022). Here, the LARS is a customized lifting crane mounted in the mother ship, lifting a docking frame designed to capture and release the AUV from above. The recovery procedure with this setup is to position the mother ship next to the AUV that is lying dead in the water and lowering the docking frame in order to capture and hoist the AUV on board.

Sarda and Dhanak (2017) present a method for AUV recovery using a catamaran USV that has a suspended winch which that carries a wing which the AUV latches on to.

Breivik and Loberg (2011) propose and demonstrate an under-way docking procedure where a USV docks to a larger mother ship. Although this procedure is designed to bring together two surface vessels, the method is useful in bringing two vessels close together at sea. The procedure comprises three phases during which the mother ship travels on the straight line, and the USV

1. tracks the mother ship until it is within a certain distance,
2. moves on a circle around the mothership until it reaches a desired bearing, and
3. reduces the distance in order to facilitate physical berthing.

The procedure, especially the first two phases, has inspired the AUV recovery method presented in this report.

1.4 Contributions

The main contributions of this report and the work it describes are summarized here:

- Development and testing of software solutions that interface and monitor the *Stinger* LARS.
- Development of a method for underway AUV recovery in four phases, tested in several full-scale experiments.
- Development and testing methods for determining the relative position of the AUV from the USV using a lidar sensor.
- Identification of physical and control related challenges related to AUV recovery in general.
- Suggestions for further development and exploration related to AUV operations in the domain of NMCM.

[2]The competition website is available at `https://www.xprize.org/prizes/ocean-discovery` (accessed June 10, 2022).

1.5 Outline

The remainder of this report is structured as follows. The design and workings of the *Stinger* LARS is described in Chapter 2. A description of the decision autonomy for the recovery method is found in Chapter 3. Details on how we detect and track the AUV using a lidar is presented in Chapter 4. Results from the most recent experimental testing with the AUV *Hugin* are detailed in Chapter 5. Chapter 6 provides our conclusions, as well as suggestions for further work and suggestions for changes to the physical setup.

2 The *Stinger* LARS

The *Stinger* is a lightweight launch and recovery system (LARS) made by *H. Henriksen Mek. Verksted* in Tønsberg, Norway. It is used for launch and recovery of the *Hugin* AUV, as well as for transportation and storage between its missions. Deployable by any vessel capable of supporting its weight and that of the AUV, it is suitable for smaller vessels such as USVs.

The system can be seen deployed on the USV *Frigg* in Figure 2.1. It consists of a structure fixed onto the USV upon which a movable trolley carries the AUV.

One key feature of the system is its use of a winch line connected to a remotely controlled hook that is fitted into the nose of the AUV being deployed. This winch line moves simultaneously with the trolley, thus securing the AUV during launch and recovery.

Upon launch, the carrier trolley is moved horizontally towards the stern of the USV. While nearing its fully aft position, the trolley starts to tilt and positions its lower end just below the water surface. At this point the remotely controlled nose hook of the AUV is triggered, and the retaining winch line is thus released. This enables the AUV to slide down along the carrier and into water to begin its work. Figure 2.2 shows the AUV ready for release.

Recovery of the AUV is possible in active sea conditions regardless of whether it is under power or not. The USV will position itself at a safe distance from where the AUV surfaces with the *Stinger* trolley extended horizontally out over the water surface. As the USV comes closer to the AUV, the trolley is moved to its fully aft position where it stays tilted with its lower end well below the water surface. Figure 2.3 shows this situation. The capture opening is 1.28 m wide, and *Hugin*'s diameter is 0.75 m with a rounded nose.

The USV is maneuvered so that the nose of the AUV moves onto the extended *Stinger* carrier, where the hook on its nose automatically captures the winch line. Figure 2.4 shows the winch line details.

After catching the nose hook, the winch line is used to pull the AUV out of the water and up onto the carrier trolley, which is then retracted back to its normal inboard deck position.

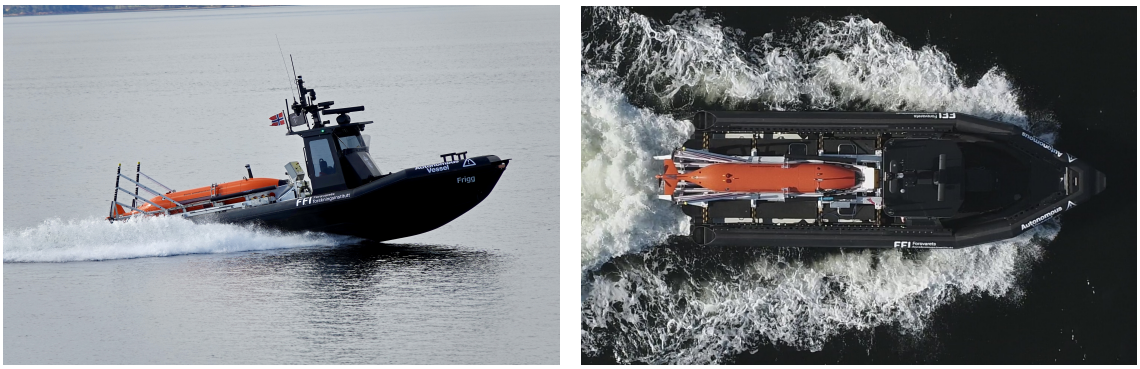

Figure 2.1 Stinger *LARS on the* Frigg *USV with the* Hugin *AUV.*

Figure 2.2 Stinger *in* `Launch` *position with its carrier extended, ready to release the AUV.*

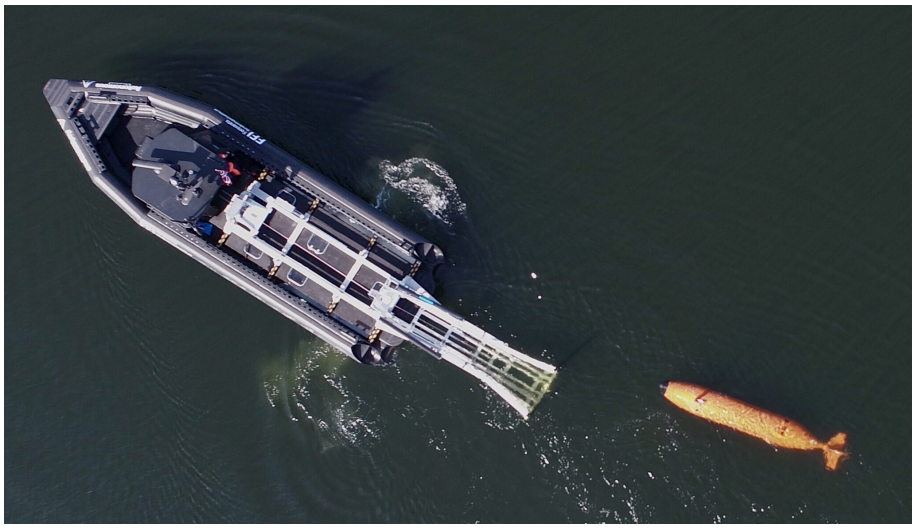

Figure 2.3 Stinger *in* `Recovery` *position with its carrier fully extended, ready to catch the AUV.*

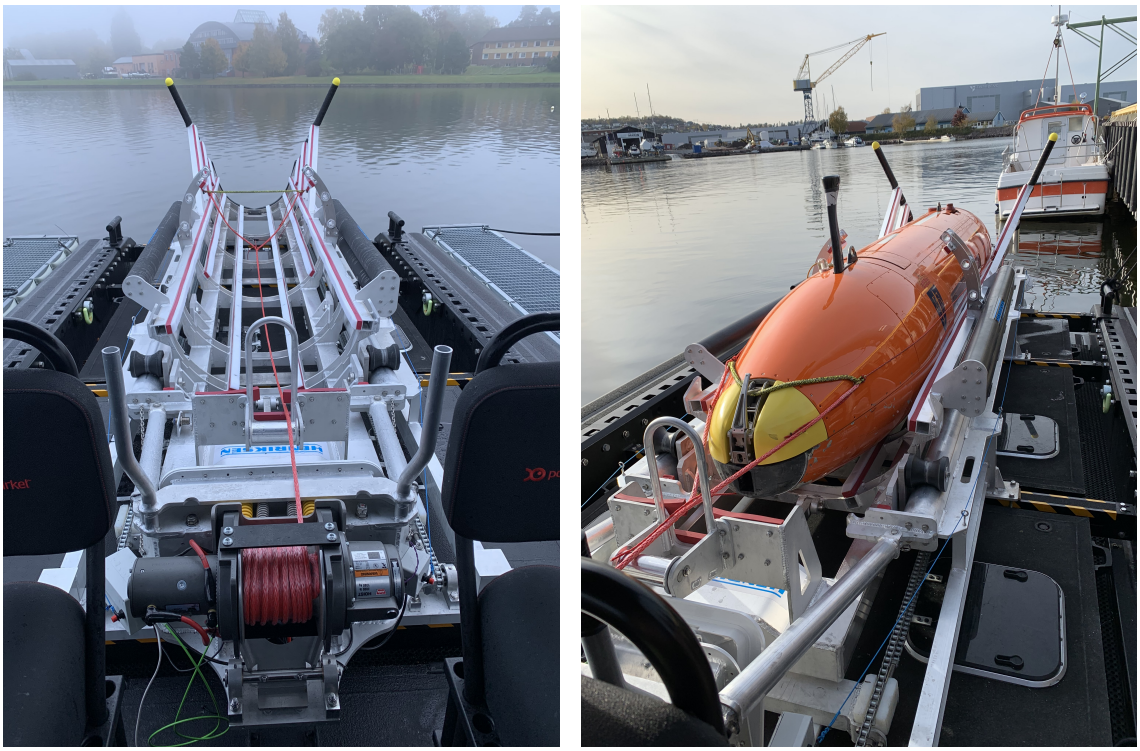

(a) Winch line (yellow rear part) will catch the nose hook during recovery.

(b) Winch line (yellow part) caught in the nose hook.

Figure 2.4 Stinger *winch line details and AUV nose hook.*

2.1 Control software

FFI has developed software to interface the *Stinger* LARS with the USV's autonomy framework HAL. This interface is based on Robot Operating System (ROS) and is named `sting_ros`. The `sting_ros` module communicates with the programmable logic controller (PLC) integrated in *Stinger* over the Ethernet-based protocol *Modbus-TCP*.

Control of *Stinger* is implemented as a state-machine with the following states:

1. `Pre recovery`: Trolley extended horizontally above the water surface.
2. `Recovery`: Trolley extended fully aft, well below water surface.
3. `Launch`: Trolley extended near full aft position, lower end just below the water surface.
4. `Start without Hugin`: Empty trolley retracted to inboard deck position.
5. `Start with Hugin`: Trolley carrying AUV retracted to inboard deck position.
6. `Manual control`: Manual control of the winch line and/or trolley.
7. `Service position`: Trolley in an inboard position that is favorable for maintenance.
8. `Idle`: Trolley in normal inboard deck position.

The state machine with transitions is illustrated in Figure 2.5.

The following actions are possible in `Manual control`:

1. Move winch line in.
2. Move winch line out.
3. Move trolley in.
4. Move trolley out.
5. Move winch line and trolley in.
6. Move winch line and trolley out.

2.2 Graphical user interface

Although the *Stinger* comes with its own physical panel for manual control by a human operator, a Graphical User Interface (GUI) for Windows has been developed by FFI for remote control and monitoring. The GUI has been used for testing the control software but can also be used for operating the *Stinger* manually from a computer or monitoring it remotely via Ethernet over radio link. The GUI has two views; the normal state machine view as seen in Figure 2.6a and the manual mode view seen in Figure 2.6b. Note that live feed from a camera overlooking the *Stinger* can be viewed in the GUI as well (see upper right-hand side of Figure 2.6a). The camera feed view can be resized along with the rest of the GUI or viewed in a separate resizable window.

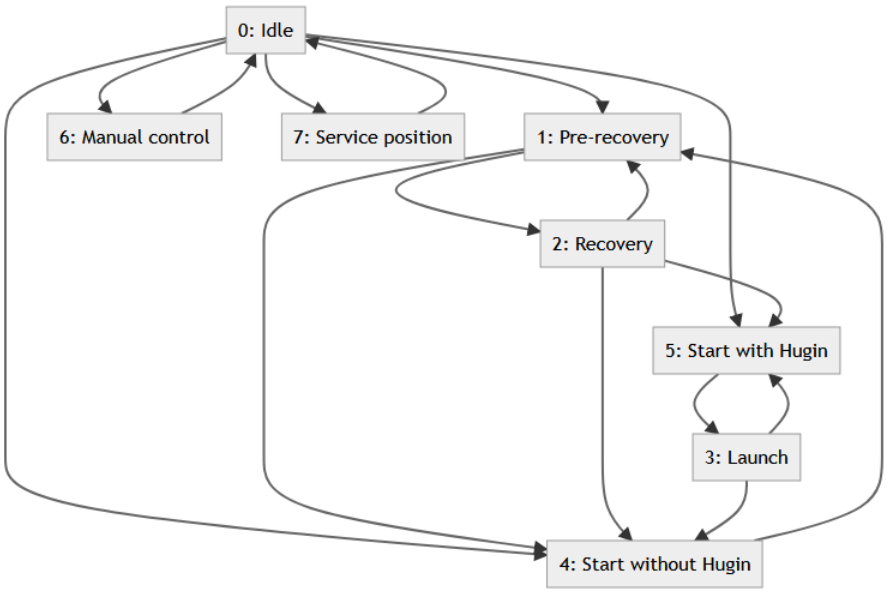

Figure 2.5 Stinger *control state machine.*

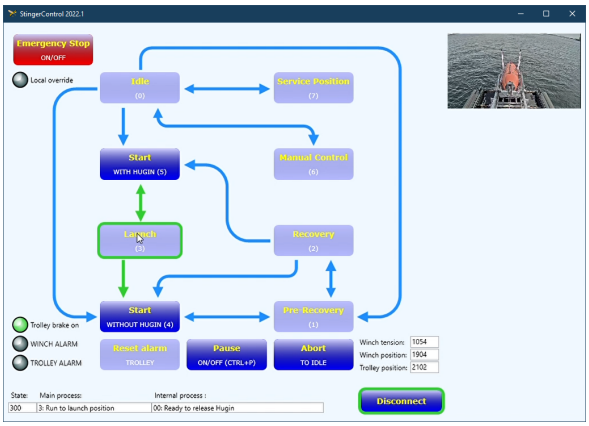

(a) Normal control with state selection.

(b) Direct manual control of winch line and trolley.

Figure 2.6 GUI for controlling the Stinger *LARS.*

3 Recovery method

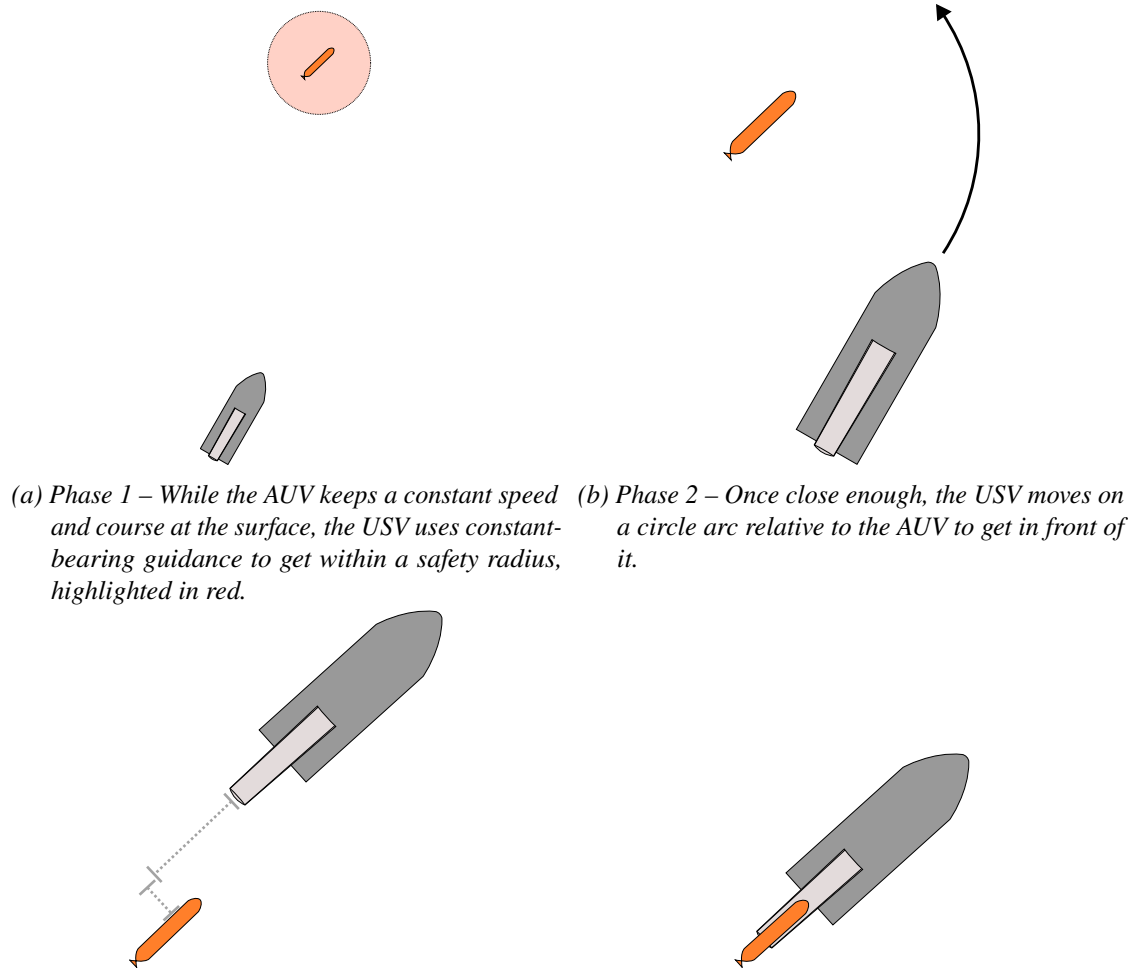

(a) Phase 1 – While the AUV keeps a constant speed and course at the surface, the USV uses constant-bearing guidance to get within a safety radius, highlighted in red.

(b) Phase 2 – Once close enough, the USV moves on a circle arc relative to the AUV to get in front of it.

(c) Phase 3 – When the USV is ahead, it spends time stabilizing the lateral offset from the AUV, simultaneously reducing the longitudinal distance.

(d) Phase 4 – When the distances are within specified tolerances, the USV quickly stops so the AUV can slide onto the LARS.

Figure 3.1 A high-level illustration of the four phases in the underway recovery method.

The method we have developed for automatic underway recovery of the Hugin AUV is inspired by the work in (Breivik and Loberg, 2011). The recovery process is divided into four phases which are tasks that are performed by the USV while the AUV is commanded to keep a constant course and speed:

Phase 1 Follow the AUV from afar, reducing the distance to a desired safety radius.

Phase 2 Position the USV in front of the AUV.

Phase 3 Stay in front of the AUV while reducing the lateral offset as much as possible. Simultaneously reduce the longitudinal distance to the AUV.

Phase 4 Stop the USV, so the AUV slides onto the aft-mounted LARS.

These phases are illustrated in Figure 3.1. From a motion control perspective, the recovery task is

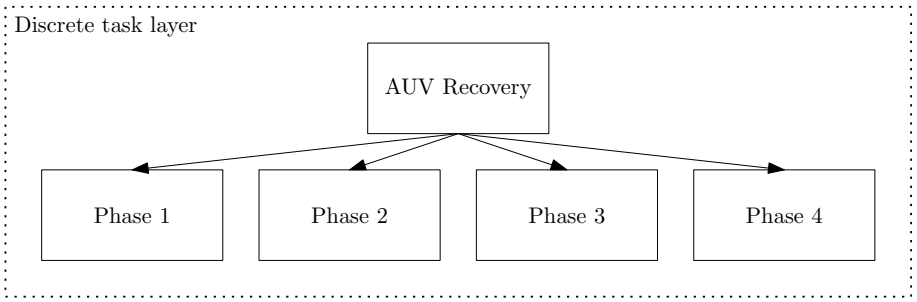

Figure 3.2 The four phases of underway recovery implemented in HAL.

now completed. However, the AUV also has to be pulled onto the bed of the USV using the Stinger LARS.

The phases above are implemented in HAL as a top-level task with four children that are traversed sequentially. See Figure 3.2.

3.1 Notation and symbols

The rest of this chapter contains calculations used in the recovery task. Table 3.1 describes the symbols used in those calculations. Positions are described with vectors placed in a reference frame, e.g.,

$$\boldsymbol{p}_a^n \tag{3.1}$$

is the position of the AUV $(\cdot)_a$ in the north-east-down (NED) $(\cdot)^n$ reference frame. Velocities are denoted

$$\boldsymbol{v}_{a/b}^n\,, \tag{3.2}$$

which means the velocity of the AUV $(\cdot)_a$ relative to the *body* reference frame $(\cdot)_{\cdot/b}$ described in the NED $(\cdot)^n$ reference frame.

Table 3.1 Symbols used in Chapter 3.

$\hat{(\cdot)}$	unit vector of the operand
$(\cdot)^n$	the north-east-down (NED) reference frame
$(\cdot)^b$	the *body* reference frame of the USV
$(\cdot)^t$	the *task* reference frame
$\boldsymbol{p}_t^n$	point to be followed with constant bearing guidance
$\boldsymbol{v}_{t/n}^n$	velocity of the point to be followed
R	safety circle radius
$\boldsymbol{p}_a^n$	AUV position
$\boldsymbol{v}_{a/n}^n$	AUV velocity
$\boldsymbol{p}_a^t$	AUV position in the *task* reference frame
$\boldsymbol{v}_{a/b}^t$	AUV velocity relative to the USV's body frame expressed in the *task* reference frame
χ_a	AUV course
$\bar{\chi}_a$	AUV commanded course
$\boldsymbol{p}_o^n$	USV (ownship) position
$\boldsymbol{v}_o^n$	USV velocity
ψ_o	USV heading
$\boldsymbol{u}_{ao}^n$	vector from $\boldsymbol{p}_a^n$ to $\boldsymbol{p}_o^n$
ϕ	relative bearing angle from the AUV to the USV
β	blind-zone angle behind the AUV
$\boldsymbol{v}_{ap}^n$	approach velocity in constant bearing guidance
$\boldsymbol{v}_{d/n}^n$	desired velocity of the USV
U_d	desired speed of the USV (magnitude of $\boldsymbol{v}_{d/n}^n$)
χ_d	desired course of the USV (direction of $\boldsymbol{v}_{d/n}^n$)

3.2 Phase 1: Following

In this phase the AUV reports its position and velocity via a ultra high frequency (UHF) link to the USV. The AUV keeps a constant speed and course at the water surface, and the USV follows the closest point on a safety-circle around the AUV using a constant bearing guidance method.

3.2.1 Circle projection

To ensure that the USV does not collide with the AUV, instead of following the AUV directly, we follow a point $\boldsymbol{p}_t$ offset from it, i.e., the closest point on a circle with the safety radius R around the AUV position $\boldsymbol{p}_a$. This section details that projection, and the calculations are carried out in the NED reference frame.

We generate a vector from the AUV to the USV

$$\boldsymbol{u}_{ao}^n = \boldsymbol{p}_o^n - \boldsymbol{p}_a^n \,, \tag{3.3}$$

where $\boldsymbol{p}_o^n$ is the ownship's position, i.e., the position of the USV. The followed point is then

$$\boldsymbol{p}_t^n = \boldsymbol{p}_a^n + R \cdot \hat{\boldsymbol{u}}_{ao}^n \,, \tag{3.4}$$

where $\hat{(\cdot)}$ denotes the unit vector.

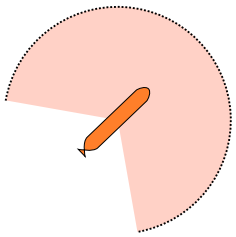

Figure 3.3 Circle projection with removed aft sector.

To avoid collision, the most important part is not to make the USV head directly to the opposite side of the AUV. However, it is unnecessary to target the safety circle directly *behind* the AUV. Much time in Phase 2 is saved by removing the aft sector of the AUV's safety circle, allowing the USV a shorter path to get in front of the AUV. This is illustrated in Figure 3.3. Instead of calculating $\boldsymbol{u}_{ao}$ as in (3.3), we calculate the relative bearing between the AUV and USV:

$$\phi = \angle(\boldsymbol{u}_{ao}^n) - \chi_a \,, \tag{3.5}$$

where $\angle(\cdot)$ denotes the angle of the vector in relation to north, and χ_a is the AUV's course. If this bearing is within the aft sector, we set the relative bearing to the angle closest to one of the edges of the sector. E.g., if the aft sector is defined to be an angle β off a line straight behind the AUV, the new relative bearing will be whichever angle of $\pi \pm \beta$ that is closest to the original bearing ϕ. The new bearing is denoted $\bar{\phi}$, and is defined by

$$\bar{\phi} = \begin{cases} \phi, & \text{if } \phi \notin (\pi - \beta, \pi + \beta) \\ \pi + \beta, & \text{if } \phi > \pi \\ \pi - \beta, & \text{otherwise.} \end{cases} \tag{3.6}$$

Instead of using $\hat{\boldsymbol{u}}_{ao}^n$ in (3.4), we use

$$\bar{\boldsymbol{u}}_{ao}^n = \begin{bmatrix} \cos(\bar{\phi} + \chi_a) \\ \sin(\bar{\phi} + \chi_a) \end{bmatrix}. \tag{3.7}$$

3.2.2 Constant bearing guidance

To follow this point, the USV controls its velocity using a constant bearing guidance method, which takes its own position $\boldsymbol{p}_o^n$, as well as the target point position $\boldsymbol{p}_t^n$, and the target point's velocity. We set the target point's velocity $\boldsymbol{v}_{t/n}^n$ equal to the AUV's velocity $\boldsymbol{v}_{a/n}^n$, since we do not expect that point to have any significant acceleration.

The constant bearing guidance method has two tunable parameters, which are

- $U_{ap} > 0$, the maximum approach speed, and
- $d_c > 0$, the characteristic transient distance, where higher values reduces speed further away from the target point.

The approach velocity is

$$\boldsymbol{v}_{ap}^n = \frac{U_{ap} \cdot (\boldsymbol{p}_t^n - \boldsymbol{p}_o^n)}{\sqrt{\left\|\boldsymbol{p}_t^n - \boldsymbol{p}_o^n\right\|^2 + d_c^2}}, \tag{3.8}$$

and is added to the AUV's velocity. The sum is fed to low-level controllers that are responsible for maintaining the desired speed and course:

$$\boldsymbol{v}_{d/n}^n = \boldsymbol{v}_{t/n}^n + \boldsymbol{v}_{ap}^n \,. \tag{3.9}$$

3.2.3 Switching conditions

The Phase 1 task is considered complete when the ownship's position is within a tolerance of the target point position, and when the ownship's velocity is within a tolerance of the AUV's velocity.

3.3 Phase 2: Positioning

This phase is responsible for positioning the USV in front of the AUV. As in Phase 1, the AUV reports its position and velocity and maintains a constant course and speed. The constant bearing guidance from Section 3.2.2 is also used to follow a point at a distance R from the AUV. However, the point is now moving on a circle arc around the AUV until it is in front.

3.3.1 Bearing dynamics

The USV is moved in front of the AUV by moving the reference point $\boldsymbol{p}_t$ on a circle arc from the USV's current position until the relative bearing ϕ is close to zero. The desired relative bearing is denoted $\bar{\phi}$, and a trajectory from its current value towards zero is generated using the following procedure:

- The desired relative bearing is converted to an arc length based on the safety radius

$$\bar{r} = R \cdot \bar{\phi} \,.$$

- We place constraints on the velocity and acceleration of $\bar{r}$.
- The shortest-time trajectory from the initial arc length $r = R \cdot \phi$ to zero is generated.
- This is converted back to a trajectory of $\bar{\phi}$ and its derivative from the initial value ϕ to zero, denoted

$$\bar{\phi}(t), \dot{\bar{\phi}}(t) \,. \tag{3.10}$$

- These values are used to calculate the follow-position and velocity:

$$\boldsymbol{p}_t^n = \boldsymbol{p}_a^n + R \cdot \begin{bmatrix} \cos(\chi_a + \bar{\phi}) \\ \sin(\chi_a + \bar{\phi}) \end{bmatrix}, \text{ and} \tag{3.11}$$

$$\boldsymbol{v}_{t/n}^n = \boldsymbol{v}_{a/n}^n + R \cdot \dot{\bar{\phi}} \cdot \begin{bmatrix} -\sin(\chi_a + \bar{\phi}) \\ \cos(\chi_a + \bar{\phi}) \end{bmatrix}. \tag{3.12}$$

As in Phase 1, these values are fed to the constant bearing guidance algorithm, where the output is sent to the low-level controllers.

3.3.2 Switching conditions

The task is considered complete when the magnitude of the actual relative bearing $|\phi|$ is below a given tolerance. If the ownship position $\boldsymbol{p}_o^n$ differs significantly from the follow-position $\boldsymbol{p}_t^n$, the trajectories in (3.10) are reset.

3.4 Phase 3: Adjustment

This phase is responsible for adjusting the USV's longitudinal distance in front of the AUV, as well as reducing and stabilizing the lateral offset between the two vessels. Longitudinal distance control is achieved through proportional-derivative (PD) control of the USV's desired speed. Lateral offset control is achieved through a relative integral line of sight (ILOS) guidance method, controlling the USV's desired course. The relative position of the AUV, as well as its velocity, is estimated through the use of a lidar mounted to the USV. More details on this estimation is available in Chapter 4.

The LARS is commanded to achieve its `Pre recovery` state when entering Phase 3. This sends the LARS bed towards the stern of the USV but maintains its height above the water. The result is a shorter path to a full `Recovery` state, first entered in Phase 4, where the LARS bed is submerged. See Chapter 2 and Section 2.1 for more information about the LARS and its states.

There have been two previous iterations of this phase. They are listed here, but the details are not included in the report, since the current iteration seems to be superior. It is also worth noting that under these iterations, we did not have a working lidar tracker, we and were limited to using the AUV's telemetry over radio, which was discontinuous and too inaccurate. An overview of the previous iterations:

- Instead of independently controlling the longitudinal and lateral distances with two separate control methods, the constant bearing guidance from Section 3.2.2 was also used here, following a point projected in front of the AUV. The AUV was tasked to follow a line, in contrast to keeping a constant course. This method was susceptible to large variations in the position of the followed point due to heading fluctuation for the AUV.
- The second iteration was similar to the current iteration, but without relative position and velocity information. The AUV was tasked to follow a line, and the AUV used the ILOS guidance method to follow the same line, offset by the reported line offset of the AUV. This method was susceptible to discontinuous and low-resolution offset information of the AUV, which made the lateral error large and hard to reduce.

3.4.1 Defining and measuring longitudinal and lateral offset

The AUV is tasked to autonomously keep a constant course, $\bar{\chi}_a$. This angle is used as the orientation of the *task* reference frame, denoted $(\cdot)^t$, whose origin is at the center of the USV, i.e., $\boldsymbol{p}_o^n$. An illustration of this reference frame is provided in Figure 3.4. When the USV and the AUV have headings aligned with $\bar{\chi}_a$, we can describe the longitudinal and lateral offsets:

- Longitudinal offset, x_a^t, is the distance from the USV to the AUV along the first axis of the task frame, and is negative when the AUV is behind the USV.
- Lateral offset, y_a^t, is the distance along the second axis of the task frame, and is positive when the AUV is to the right of the USV.

This reference frame is used for two reasons:

- The *task* frame has a constant orientation, as opposed to, e.g., the USV's *body* frame. Since the USV's heading is actively used in controlling lateral offset, using the *body* frame would cause unwanted oscillations.
- Since the *task* frame is based on the AUV's desired course, the current *lateral* offset in the *task* frame predicts a future lateral offset in the USV's *body* frame when *longitudinal* distance is reduced, assuming that

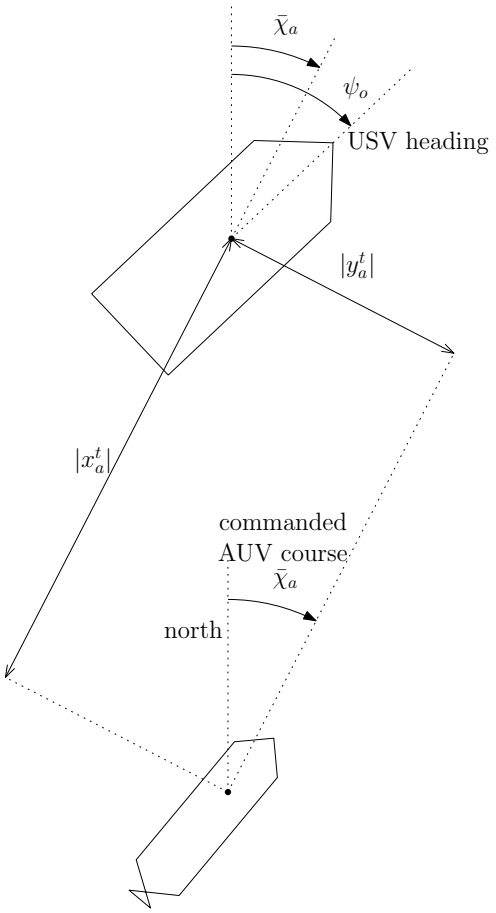

Figure 3.4 Illustration of the task *reference frame, defined by the USV's origin and the AUV's commanded course.*

1. the AUV is able to follow the desired course, and
2. the USV's heading is not significantly disturbed.

This is key in Phase 4, where we want the AUV to hit the center of the USV after the USV comes to a halt.

Distance estimates from the USV to the AUV are given in the USV's body frame $(\cdot)^b$, so we must transform the measurements $\boldsymbol{p}_a^b$ to $\boldsymbol{p}_a^t$:

$$\boldsymbol{p}_a^t = \begin{bmatrix} x_a^t \\ y_a^t \end{bmatrix} = \mathbf{R}_b^t(\psi_o) \cdot \boldsymbol{p}_a^b \,, \tag{3.13}$$

where

$$\mathbf{R}_b^t(\psi_o) = \begin{bmatrix} \cos(\bar{\chi}_a - \psi_o) & \sin(\bar{\chi}_a - \psi_o) \\ -\sin(\bar{\chi}_a - \psi_o) & \cos(\bar{\chi}_a - \psi_o) \end{bmatrix}, \tag{3.14}$$

ψ_o is the USV's heading, and

$$\boldsymbol{p}_a^b = \begin{bmatrix} x_a^b \\ y_a^b \end{bmatrix}. \tag{3.15}$$

Velocity estimates of the AUV, $\boldsymbol{v}^b_{a/n}$, are also available in the USV's body frame, i.e., with the relationship

$$\dot{\boldsymbol{p}}^t_a = \boldsymbol{v}^t_{a/b} = \begin{bmatrix} \dot{x}^t_a \\ \dot{y}^t_a \end{bmatrix} = \mathbf{R}^t_b(\psi_o) \cdot (\boldsymbol{v}^b_{a/n} - \boldsymbol{v}^b_{o/n}) \,. \tag{3.16}$$

The AUV's velocity relative to NED in the task frame is

$$\boldsymbol{v}^t_{a/n} = \begin{bmatrix} u^t_{a/n} \\ v^t_{a/n} \end{bmatrix} = \mathbf{R}^t_b(\psi_o) \cdot \boldsymbol{v}^b_{a/n} \,. \tag{3.17}$$

3.4.2 Controlling longitudinal distance

During Phase 3, we want to be able to reduce the longitudinal distance x^t_a to make the braking distance in Phase 4 shorter. The desired distance is denoted $\bar{x}$ and is an operator input to HAL, low-pass filtered to avoid large, sudden changes. The distance is achieved by controlling the USV's desired speed U_d using a PD controller:

$$U_d = u^t_{a/n} - K_p \cdot (x^t_a - \bar{x}) - K_d \cdot \dot{x}^t_a \,, \tag{3.18}$$

where

- $K_p > 0$ is the proportional gain, and
- $K_d > 0$ is the derivative gain.

3.4.3 Controlling lateral offset with relative ILOS guidance

Lateral offset is controlled by applying an ILOS guidance law to the USV's course. The goal of that control law is to reduce lateral offset y^t_a to zero. The use of ILOS for straight-line path following is extensively covered in (Borhaug, Pavlov and Pettersen, 2008) and (Caharija et al., 2016).

The desired course is set to

$$\chi_d = \bar{\chi}_a + \arctan \frac{d}{\Delta} \,, \tag{3.19}$$

where

$$d = y^t_a + \int C_i \cdot y^t_a \, \mathrm{d}\tau + C_d \cdot \dot{y}^t_a \,. \tag{3.20}$$

- $\Delta > 0$ is the lookahead distance of the ILOS guidance law,
- $C_i \geq 0$ is the integral gain, and
- $C_d \geq 0$ is the derivative gain.

The integral term is clamped to avoid windup issues.

3.4.4 Switching conditions

This phase lasts until an operator sends a special command to HAL, before switching to Phase 4.

3.5 Phase 4: Braking

When entering this phase, the LARS is commanded to its `Recovery` state, which submerges the bed under water behind the USV. The USV is commanded to come to a halt without changing its heading, allowing the AUV to slide onto the LARS bed.

4 Detection and tracking of the AUV

This chapter elaborates upon the topic of tracking the relative position and velocity of the AUV using lidar measurements, as motivated in the earlier description of Phase 3.

A very similar application is described in (Rundhovde et al., 2022), which covers tracking of a co-operative vessel in autonomous mine sweeping operations using USVs, also employing a lidar for detection. The report describes relevant parts of the software that provide situational awareness (SA) to the on-board autonomy system on *Frigg* and *Odin* and covers the foundation and motivation of the chosen method in greater detail. Hence, we refer to that report for background information when we in the following describe the method of tracking the AUV using lidar.

4.1 Sensors

We have decided to use lidar as the primary sensor for range measurements. Lidars determine range by illuminating an object or a surface with a laser and measuring the time for the reflected light to return to the receiver.

Frigg was initially equipped with a OS2-128 lidar from *Ouster*,[3] but it is mounted in such a way that it has a limited view towards the aft. We have therefore installed an additional OS1-64 lidar to complement in this main area of interest. Both lidars are capable of scanning 360° at 10 or 20 Hz, but the range and resolution differ between the models. The OS2 is rated for ranges up to 240 m, with 128 lasers distributed over a 22.5° vertical field of view. The OS1 has 120 m range with 64 lasers covering 45° vertically. In our setup, the OS1 is configured with a narrowed horizontal field of view, such that only a sector of 90° around the aft is sampled. The OS2 covers 360° and will aid in keeping track of *Hugin* at longer distances. The lidars provide range measurements with centimeter precision. Additionally, each data point also contains the intensity of the reflected light and the sensors can return passive measurements of ambient near-ir light, which in practice make them applicable as low-resolution grayscale cameras.

Besides the lidars, other sensors that we rely on are an inertial navigation system (INS) and a time synchronization server. The INS measures the change in position, orientation, and velocity of the USV's *body* frame. The time synchronization server is used to synchronize clocks across the system and is required in order to fuse information from different sensors correctly. Time synchronization between the USV and the AUV rely on global navigation satellite system (GNSS).

4.2 Detecting the AUV

A complete tracking framework with a running object tracker is already available as part of the deployed SA software stack on *Frigg* (Larsen, 2022). The current system primarily uses data from a radar to track objects on the water, like boats and sea marks. As radar measurements consists only of bearing and range with no elevation, and we in any case are mainly concerned with objects on the water, tracking is performed in two dimensions on a local sea plane. We choose to utilize this existing framework also in the case of monitoring the relative position and velocity of an AUV.

A key feature of the object tracker is that tracking is performed relatively in a *body*-attached frame, which yields higher precision compared to tracking in an absolute, earth-fixed frame. Hence,

[3]Product sites for the *Ouster* OS1-64 and OS2-128 lidars, accessed May 31, 2022:
`https://ouster.com/products/scanning-lidar/os1-sensor/`,
`https://ouster.com/products/scanning-lidar/os2-sensor/`.

Figure 4.1 Retroreflective tape attached to the antenna for simplified detection with lidar.

we strive to provide the tracker with *relative* measurements. Details around the topic of absolute vs. relative coordinates is covered in (Rundhovde et al., 2022).

The chosen approach is to attach a retroreflector to the antenna of *Hugin*, as shown in Figure 4.1. Since retroreflectors will reflect laser beams with low absorption, the reflector can be detected by applying a threshold on the measured intensity of laser returns. Among laser returns above the chosen threshold value, we select the most intense sample and pass it on as a *relative* position measurement to the tracker. As this direct approach may give spurious detections on other highly reflective objects, we use telemetry data to filter detections. In simple terms, a lidar measurement is accepted only if it is "reasonably close" to *Hugin*'s reported position. Separately, telemetry is also utilized to provide the tracker with *absolute* position measurements. With such measurements, the AUV track can be initialized or kept alive even in the absence of lidar measurements, albeit with lower precision.

4.3 Tracking in a local sea plane

In the following sections we will go into finer details of relative tracking and the coordinate frame in which tracking is performed.

In order to take advantage of relative representations, we define three *body*-attached coordinate frames:

- The *body* frame $\mathcal{F}_b$ is fixed to the vessel body with its x-axis positive forwards, y-axis positive to the starboard, and z-axis positive downwards, commonly denoted forward-right-down (FRD). It is the same frame as denoted $(\cdot)^b$ in Section 3.1.
- The *tracker* frame $\mathcal{F}_p$ has the same origin as $\mathcal{F}_b$. The xy-plane of $\mathcal{F}_p$ is assumed fixed and parallel to the mean water surface, such that the third axis $\mathbf{e}_z^p$, is parallel to the gravity vector $\mathbf{g}$. For the sake of brevity, we call the xy-plane of $\mathcal{F}_p$ for *the P-plane*. $\mathcal{F}_p$ moves along the path of the vessel with its x-axis positive forwards, y-axis positive to the starboard, and z-axis positive downwards. Formally, the relation between $\mathcal{F}_b$ and $\mathcal{F}_p$ is

$$\mathbf{e}_x^p \triangleq \mathbf{e}_y^b \times \mathbf{g}\,. \tag{4.1}$$

- $\mathcal{F}_s$ is the lidar *sensor* frame. It can be either the OS1 or the OS2.

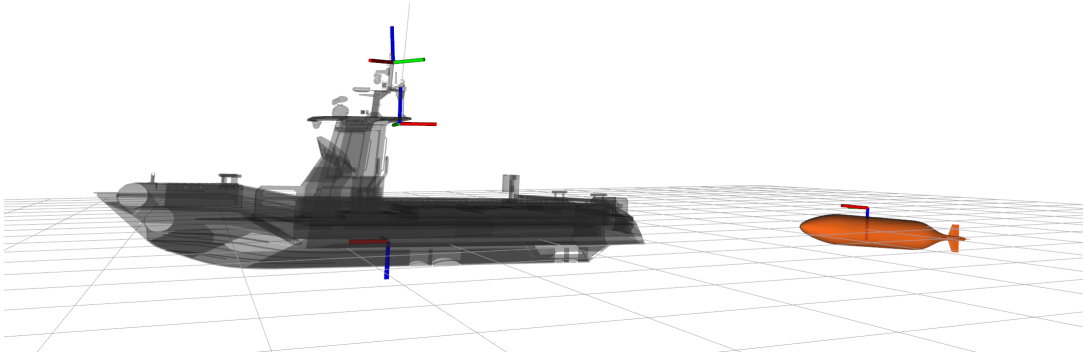

Figure 4.2 Frames that are part of tracking for AUV recovery. The frames $\mathcal{F}_p$ and $\mathcal{F}_b$ are co-located near the waterline, along the centerline of the vessel. $\mathcal{F}_{s_{os2}}$ is at the very top of the mast, while $\mathcal{F}_{s_{os1}}$ is mounted aft on the hardtop. The tracked retroreflector frame can be seen above the AUV.

Figure 4.2 shows $\mathcal{F}_b$, $\mathcal{F}_p$ and $\mathcal{F}_s$ rendered on a model of the vessel.

An advantage of using the front-oriented local P-plane compared to, e.g., a north-oriented plane is that we can do relative tracking without requiring a good measure of absolute heading. This, in turn, is a significant step towards tracking in GNSS-denied environments.

4.3.1 Adding measurements

In order to probabilistically compare a new measurement to any existing track, the tracker state must be predicted up to the same timestamp as that of the measurement. However, tracking in a *body*-attached frame complicates the logic of the tracker. Since we work with a tracker frame that moves independently in relation to what we are tracking, we must take the relative motion of $\mathcal{F}_p$ into account for each prediction of the tracker state. In practice, when we predict up to the timestamp of a new measurement, each track's position must be transformed from $\mathcal{F}_p(t_{\text{prev}})$ to $\mathcal{F}_p(t_{\text{curr}})$ in order to account for our platform's egomotion. In each timestep, we update the existing set of `tracks` with a new set of `measurements` as follows:

```
pose_p2p1 = get_relative_pose("P", prev_timestamp, curr_timestamp)

for track in tracks:
  track = track.predict(curr_timestamp)
  track = transform(pose_p2p1, track)

matches = compare(tracks, measurements)

for track, measurement in matches:
  track.update(measurement)

tracks = add_new_tracks_for_unmatched_measurements(tracks, measurements)
tracks = remove_bad_tracks(tracks)
```

Listing 4.1 Updating tracks when using a relative tracker frame

4.3.2 Detecting and tracking the AUV using relative tracking

In this section we describe the overall process that is used in tracking for AUV recovery.

Initially, a new *AUV recovery track* can only be spawned using absolute coordinates from telemetry. An AUV recovery track has a special tag that makes it possible to distinguish it from other tracks. We continue to add telemetry data as measurements to the tracker, so tracking can eventually be performed solely on absolute data. If available, remote odometry data is included in the measurements so that tracking can be improved with known values for pose and velocity. If not, position measurements alone are sufficient.

The process for detection of retroreflectors has a feedback loop from the tracker, so that it receives the current tracker state. For each new lidar detection, the tracker state gets predicted up to the current timestamp. The lidar detection is then compared to existing tracks. In order to compare, the detection must first be transformed from $\mathcal{F}_s$ to $\mathcal{F}_p$:

$$\mathbf{x}^p = \mathbf{T}_{pb}(t_{\text{curr}})\, \mathbf{T}_{bs}\, \mathbf{x}^s\,, \tag{4.2}$$

where $\mathbf{x}^s$ is the detection in $\mathcal{F}_s$, $\mathbf{T}_{bs}$ is the calibrated pose of $\mathcal{F}_s$ with respect to $\mathcal{F}_b$, $\mathbf{T}_{pb}(t_{\text{curr}})$ is the pose of $\mathcal{F}_p$ with respect to $\mathcal{F}_b$ at the specific timestamp t_{curr} of the detection, and $\mathbf{x}^p$ is the detection finally in $\mathcal{F}_p$. If a track with the special AUV recovery tag exists and the detection is reasonably close to the track's estimated position, the detection is allowed to update the track. Lidar measurements are not allowed to spawn new tracks. Since relative lidar measurements come at a high rate and have low uncertainty compared to absolute telemetry data, they may quickly relocate the track's estimated position.

The position and velocity of the AUV track is predicted and then published at a fixed rate.

5 Experiments

The development of the recovery method has been a process of continuous iteration and testing. In total, six full-scale tests and experiments have been performed on the north side of Østøya, near Horten in the Oslofjord. Here we present results from the latest experiment that were executed on May 13, 2022, with the USV *Frigg* and the AUV *Hugin*.

Remark. *The recovery method as described in Chapter 3 prescribes that* Hugin *follow a constant* course *reference. In the preliminary runs of this experiment we found that* Hugin*'s course-following mode produced significant lateral oscillations that caused trouble in the recovery process. This led us to switch to using constant* heading *reference in place of $\bar{\chi}_a$ in the data presented below.*

In this experiment, the Navy provided *Hugin* as well as operators to plan its route. *Hugin* was tasked to run on a constant heading with constant thrust to achieve ~1.7 m/s over ~1000 m. This was repeated several times to give the USV multiple chances to perform recovery. An example of *Hugin*'s mission is available in Figure 5.1. No significant environmental effects affected *Hugin* or *Frigg*, other than a near-constant ocean current in the ~0.2 m/s range.[4]

The switching from Phase 3 to Phase 4 is a manual input from an operator who is on-board *Frigg*. They judge visually whether they think the recovery attempt will be successful, based on the perceived lateral offset and stability of *Hugin* as well as *Frigg*. If it looks like *Hugin* will miss the Stinger, the operator cancels the recovery by manually increasing *Frigg*'s speed to avoid an unwanted collision. Of the four attempts made this day, three were successful, and we will present data from one of the successful attempts and from the unsuccessful one.

5.1 Successful attempt

We present position, velocity, and distance data from the four phases. Phases 1 and 2 are combined in Figure 5.2. The attempt was started when *Frigg* was quite close to *Hugin*, so Phase 1 lasted for only five seconds before the target was reached. Phase 2 brings *Frigg* nearly in front of *Hugin* before the relative bearing ϕ is within its tolerance. This tolerance is quite large because lateral offset convergence is faster during Phase 3. During Phase 2 the distance between vessels is close to 30 m for the entire duration.

Phase 3 is presented in Figure 5.3. In addition to inter-vessel distance, this plot shows the lateral displacement y_a^b. Phase 3 lasts for three minutes and covers ~320 m. The time is spent reducing longitudinal distance from 30 m to 20 m and the lateral distance to ~0.1 m in both the *body* and *task* reference frames. We can see that *Frigg* first overshoots the lateral displacement set point, which is why it takes a while to stabilize at an acceptable value. Phase 3 ends when the USV operator commands *Frigg* to enter Phase 4.

Once Phase 4 is active, *Frigg* quickly comes to a halt. This is evident from the speed plot in Figure 5.4. This plot also marks the time of collision between the vessels, and their shapes are drawn at that time. We see that at the time of collision, the lateral displacement is quite low, at ~0.1 m, which results in a successful recovery attempt.

Figure 5.5 shows details from lidar tracking of the distance from *Frigg* to *Hugin* during phases 3 and 4. The plots include uncertainty for each sensor and how the track's uncertainty is reduced with information from the lidars. The track is initiated by telemetry, but thereafter mainly follows the

[4]The ocean current was not measured during the experiments. The figure is an approximation from the weather service at `https://yr.no`.

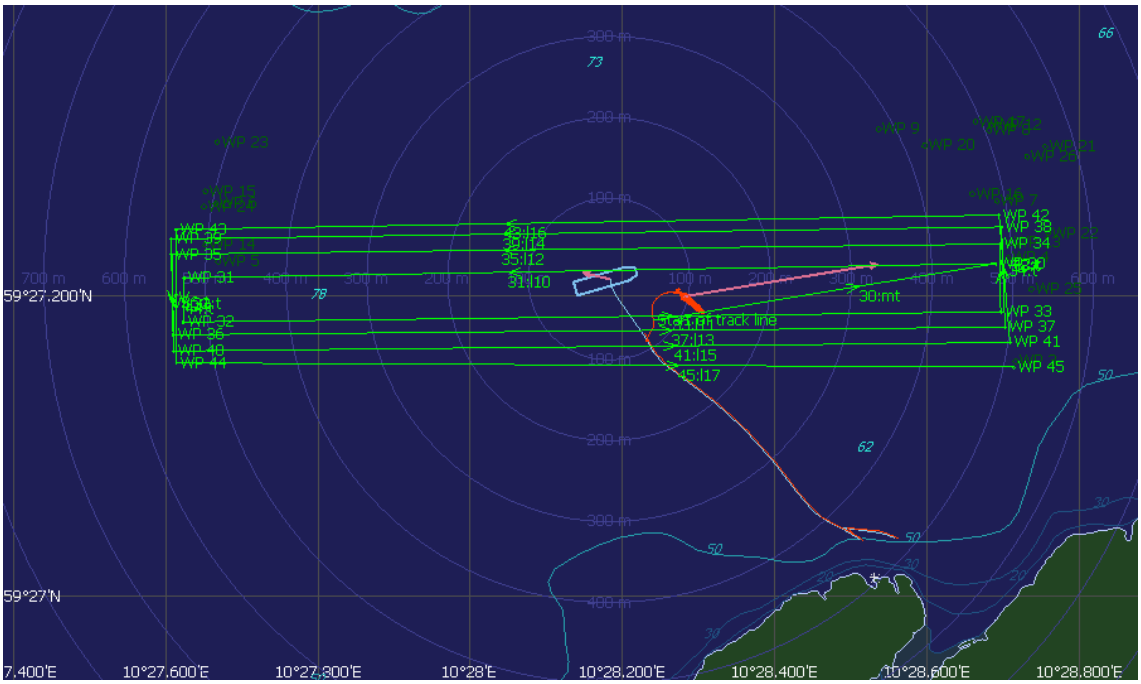

Figure 5.1 A screen capture from the Hugin *operating station, showing how* Hugin *(the orange figure) is tasked to run along the straight lines (light green).*

more precise lidar measurements. After approx. 60 s the AUV becomes observable by the OS1. When Phase 4 starts at approx. 230 s, the OS2 looses sight of the AUV. At the time of collision, no lidars are able to detect the antenna, and the track is drawn back towards telemetry measurements. Note that for illustration purposes, the track is spawned at the beginning of Phase 3. Normally, tracking is performed continuously and will initiate well ahead of any attempt of recovery.

Figure 5.6 contains links to video footage and animations from this recovery, and Figure 5.7 presents a sequence of pictures from the successful attempt.

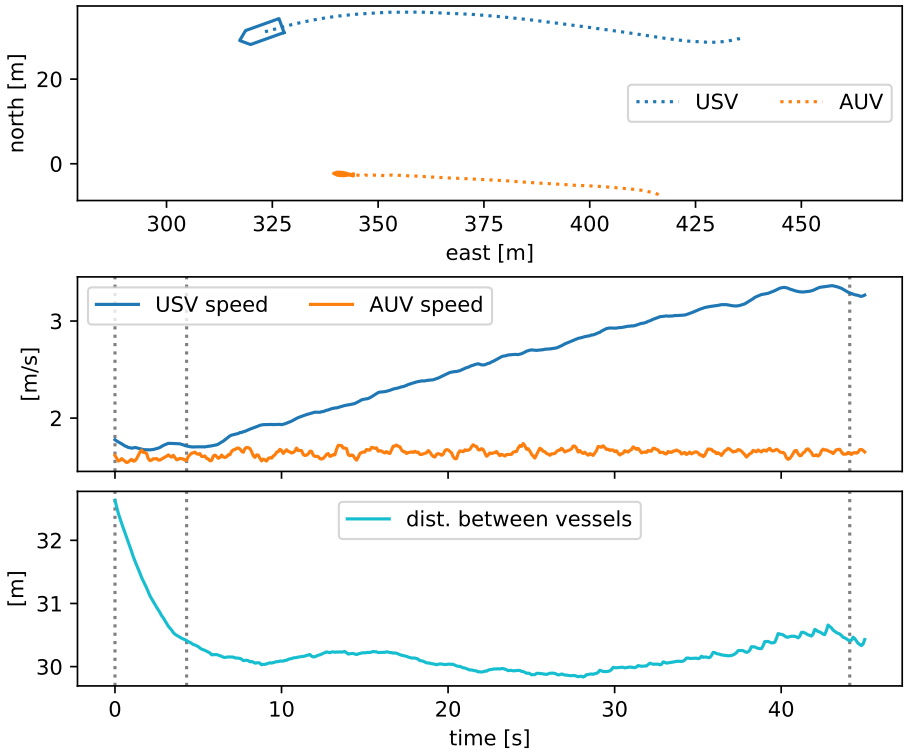

Figure 5.2 Successful attempt, phases 1 and 2. The plot shows north and east position, the speed of Frigg *and* Hugin*, as well as the distance between the vessels. Vertical gray lines mark phase transitions.*

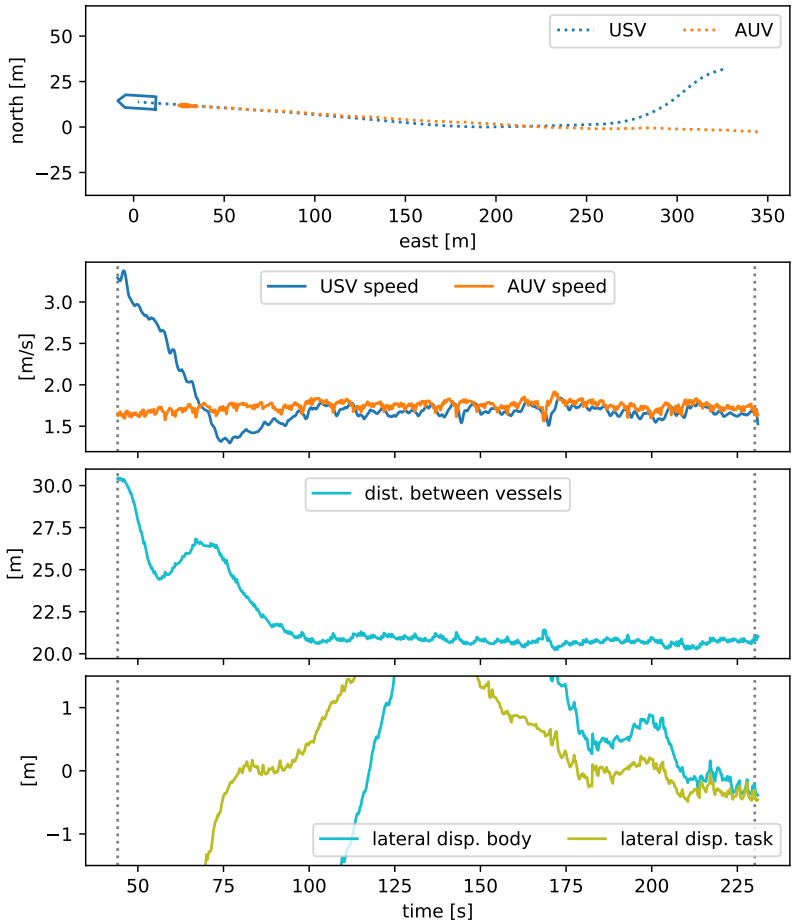

Figure 5.3 *Successful attempt, Phase 3. In addition to position, speed and inter-vessel distance, the plots shows lateral displacement in the* body *and* task *reference frames.*

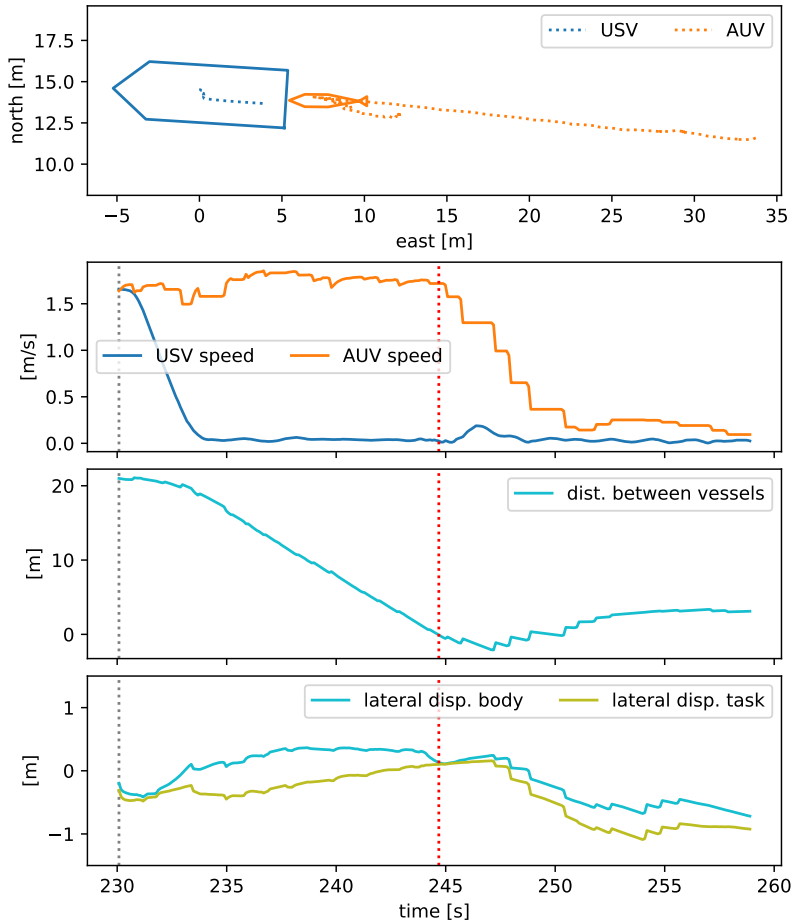

Figure 5.4 *Successful attempt, Phase 4. The vessel shapes are drawn at the time of collision, which is also marked by a red vertical line in the speed and distance plots. Time of collision is calculated from inter-vessel distance and can be slightly delayed.*

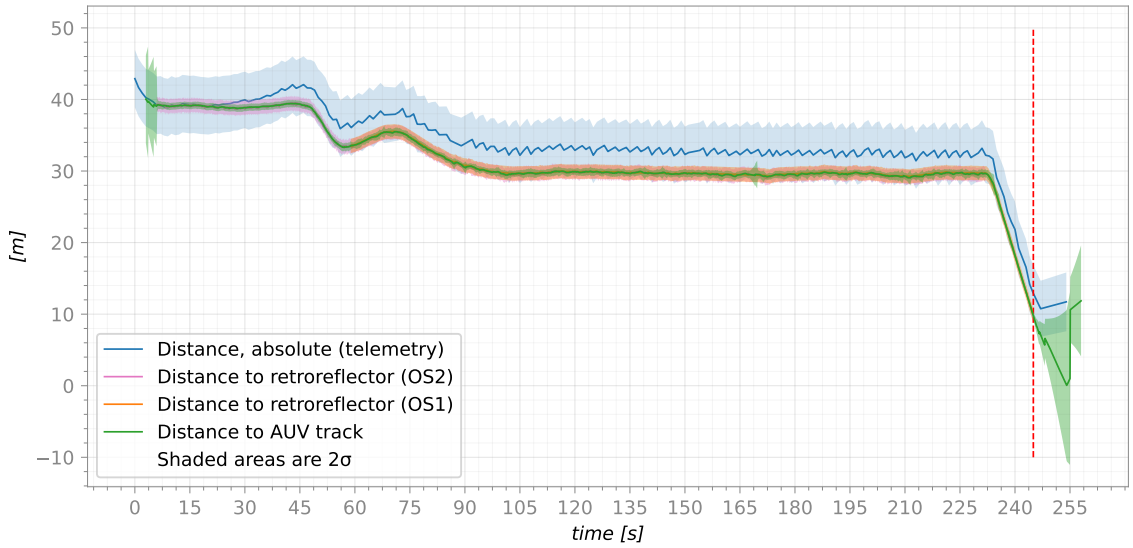

Figure 5.5 *Tracking during successful attempt, phases 3 and 4. The blue line is absolute distance based on telemetry, i.e., the distance between both vessels' GNSS measurements. The pink and yellow lines show the raw distance measurements from the lidars to the retroreflector. The green line is the result of relative tracking, and shows the distance from $\mathcal{F}_b$ to the predicted AUV track. Shaded areas in respective colors are 2σ of uncertainty around the estimate.*

(a) Footage: `https://vimeo.com/720617490`.

(b) Animations: `https://vimeo.com/720617240`.

Figure 5.6 *QR codes that link to video footage and animations from the successful recovery attempt.*

(a) End of Phase 3.

(b) Beginning of Phase 4.

(c) End of Phase 4.

(d) Recovery successfully completed.

Figure 5.7 A sequence of footage from the successful recovery attempt.

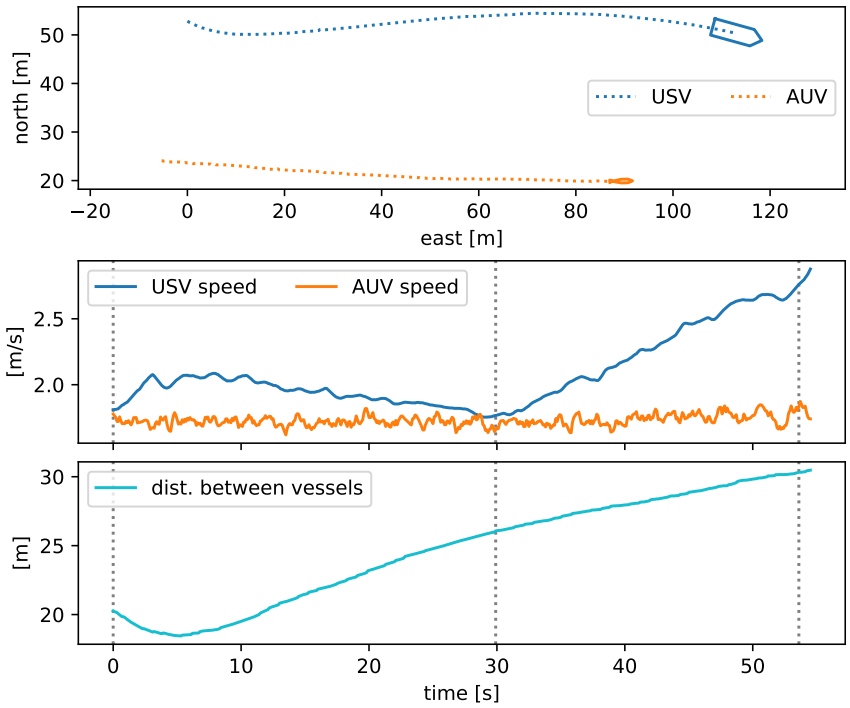

Figure 5.8 Unsuccessful attempt, phases 1 and 2.

5.2 Unsuccessful attempt

Similar to Section 5.1, we present position, velocity, and distance data from the unsuccessful attempt in figures 5.8 through 5.10. Phases 1 through 3 are very similar to the successful attempt. Phase 3 lasts for five-and-a-half minutes before Phase 4 is commanded. At that time, the lateral displacement is ~ -0.2 m in *body*, but noticeably larger at ~ -1 m, in the *task* frame. This difference is due to a discrepancy between the USV's heading angle ψ_o and the AUV's reference angle $\bar{\psi}_a$. During Phase 4, the *body* displacement drifts from ~ -0.2 m to ~ 0.9 m, which results in an unsuccessful recovery attempt and an unwanted collision. The USV operator reacts to the imminent collision by manually increasing *Frigg*'s speed to reduce the impact. Pictures from this attempt are presented in Figure 5.11.

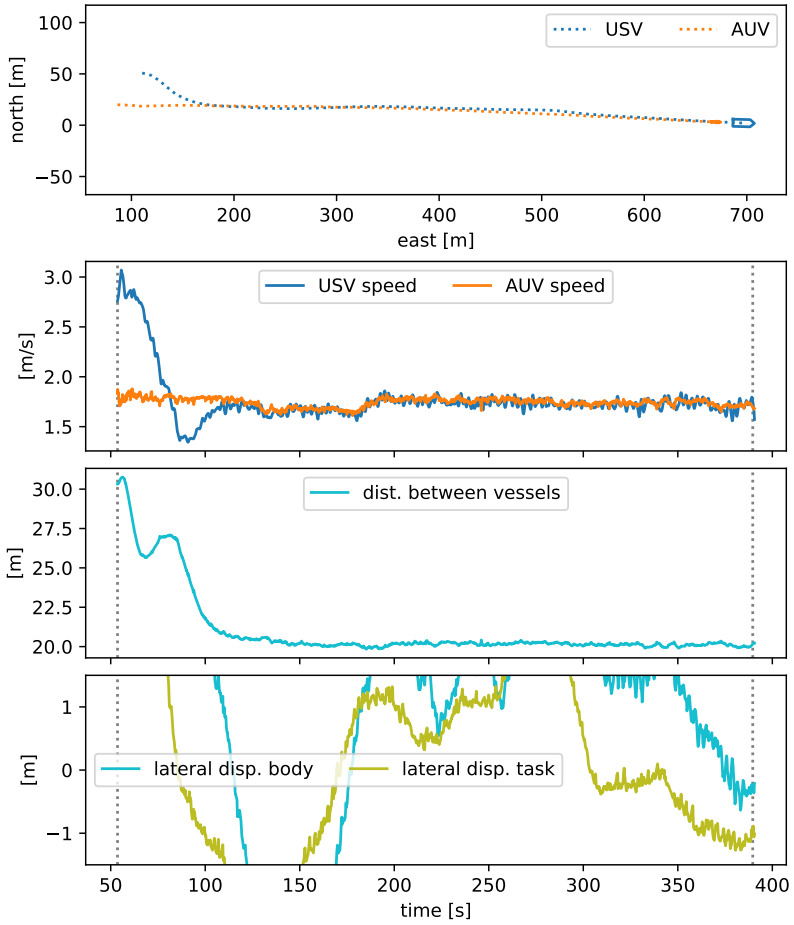

Figure 5.9 Unsuccessful attempt, Phase 3.

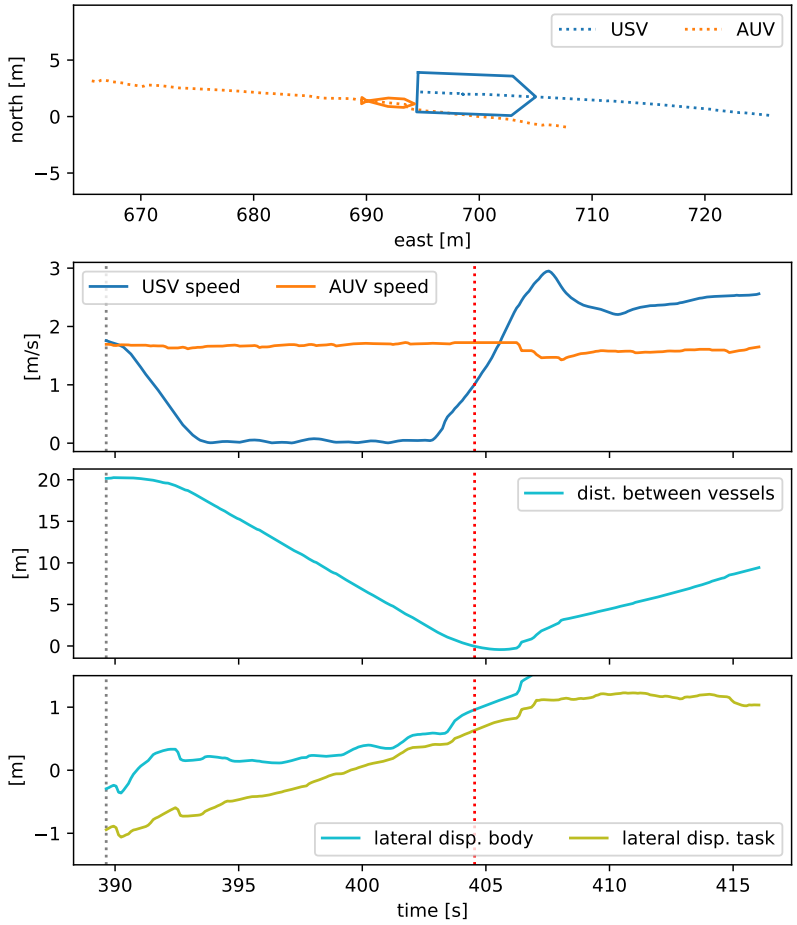

Figure 5.10 Unsuccessful attempt, Phase 4.

5.3 Discussion

Frigg is generally able to perform successful recoveries, and in this discussion we focus mainly on the differences between a successful and the unsuccessful recovery attempt. Phases 1 and 2 are quite similar for the two attempts presented above, and the behavior is typical for all the data we have gathered. I.e., *Frigg* is always able to place itself in front of *Hugin*. The differences are found in phases 3 and 4.

A characteristic of a successful recovery attempt is that the lateral *body* displacement remains small during Phase 4. If *Hugin* was able to keep a constant course, the lateral *task* displacement would predict the *body* displacement when the longitudinal distance is reduced. As we remarked in the start of this chapter, due to problems with lateral oscillations when using constant course control, we instead elected to use a constant heading approach for *Hugin*. During Phase 3 *Hugin* was greatly affected by wakes from *Frigg*'s water jets and hull, which induced lateral drift and sideslip, meaning that there is a large discrepancy between *Hugin*'s heading and course. This is highlighted in Figure 5.12, where we contrast the successful attempt to the unsuccessful attempt, and show the lateral dimensions. In the successful attempt, *Hugin*'s lateral velocity is significantly smaller than in the unsuccessful attempt, where the lateral velocity remains larger due to *Hugin*'s sideslip.

Due to the risk of impact, we decided that an operator on-board *Frigg* would decide whether a recovery attempt would be safe. The most available way they had to make this judgment is by visually controlling the alignment between the vessels. This alignment corresponds to the lateral *body* displacement, which means that the operator's prediction will be negatively affected by differences in *Frigg*'s heading and *Hugin*'s course. A software-defined indication based on a prediction of *Hugin*'s eventual lateral *body* displacement could improve the judgment call.

Hugin's diameter is 0.75 m, and a significant part of it (~15 cm to either side of its center) must hit within the *Stinger*'s capture opening for a successful capture. The capture opening is 1.28 m wide, which allows us a tolerance of only ~0.5 m to either side of center. This tolerance is for conditions where *Frigg* and *Hugin*'s headings are perfectly aligned, and the tolerance reduces with increased discrepancy.

Small tolerances, failure to tightly hold *Hugin*'s prescribed course, and discrepancies between predicted and actual lateral distances at impact are all contributing factors when a recovery attempt fails. These are areas to improve upon in further development to increase robustness of the recovery method.

(a) End of Phase 4. Hugin*'s lateral alignment is clearly too far off center.*

(b) From Hugin*'s point of view.*

Figure 5.11 Footage from the unsuccessful recovery attempt.

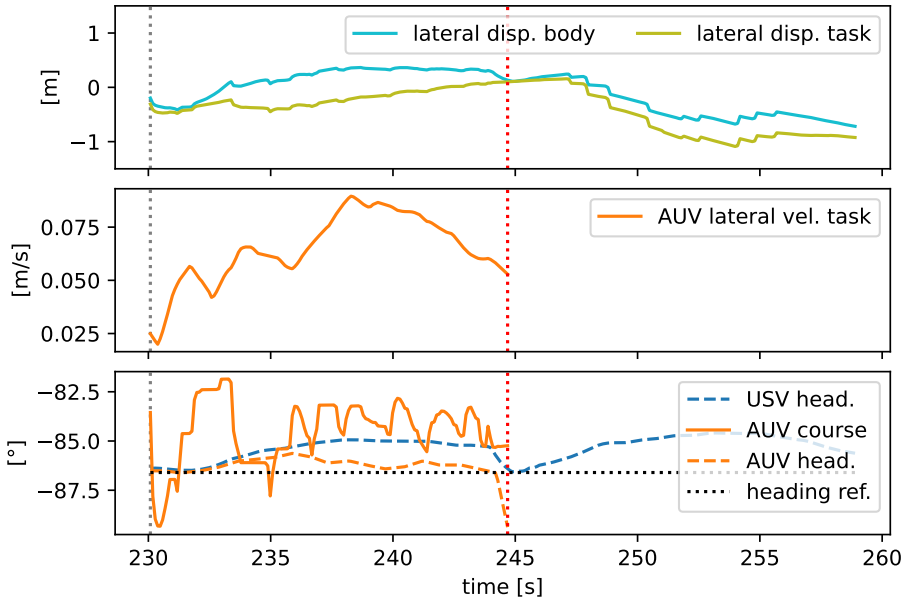

(a) Successful attempt.

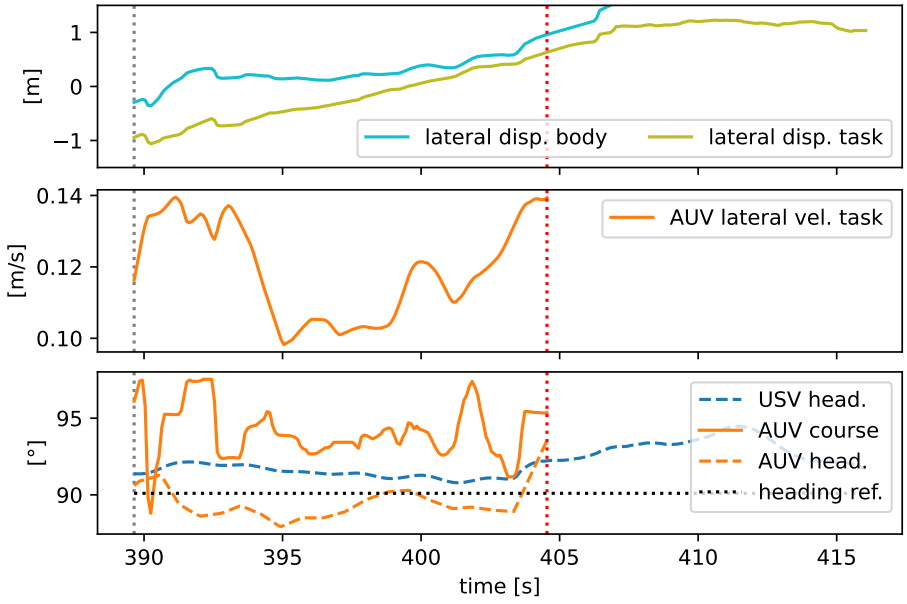

(b) Unsuccessful attempt.

Figure 5.12 Plots of lateral dimensions during Phase 4. Lateral displacements, equivalent to figures 5.4 and 5.10, as well as the AUV's lateral velocity in the task *frame, and vessel heading and course angles are plotted. The quick change in* Hugin*'s heading right before the time of collision is likely the start of the actual collision.*

6 Conclusion

As a step in exploring and developing autonomous technology for the Royal Norwegian Navy's future naval mine countermeasures (NMCM) capabilities, we present a method for underway recovery of an autonomous underwater vehicle (AUV) with an unmanned surface vehicle (USV). This method controls a *Stinger* launch and recovery system (LARS) mounted to the USV to capture the *Hugin* AUV while *Hugin* is underway. Detection and relative positioning of *Hugin* is performed by fusing telemetry from *Hugin* with data from a lidar tracker. The recovery method is divided into four phases and implemented in the decision autonomy framework Hybrid Autonomy Layer (HAL). The method is tested in several full-scale experiments, and the report presents data from a selection of recovery attempts.

The experimental results show that the current iteration of underway AUV recovery method is able to recover successfully, but that it is challenging to do this under a wide envelope of conditions. The success rate is negatively affected by lateral drift due to ocean currents or USV-AUV interactions. The method used to predict the relative position when physical contact is made between the USV and AUV is dependent on the AUV's ability to tightly follow a commanded course, which has proven difficult in practice. To successfully capture *Hugin* with the *Stinger*, *Hugin* must hit with a significant part of its nose within the *Stinger*'s capture opening. These tolerances are quite small and the lack of accurate lateral motion control for the USV makes it difficult to robustly capture the AUV.

Despite the difficulties, the underway AUV recovery method has made several successful captures, and with certain improvements, the method could be an important operational capability for the Navy in NMCM operations. Important knowledge gained during development and experiments of this method is highly relevant to development of more advanced AUV recovery methods, such as capturing *Hugin* when it is dead in the water. This includes knowledge about communication, estimation of position, velocity, and orientation, moving an USV around the AUV while minimizing the risk of collision, as well as how the LARS interacts with *Hugin* during recovery.

6.1 Further work

The following is a list of recommendations of areas to focus on when continuing the development of technology for autonomous AUV recovery. The list contains some concrete suggestions, as well as general remarks.

- Currently, the recovery method requires an on-board operator to judge whether or not a capture attempt can safely be made. We want to improve the method and build confidence in the autonomy so that this requirement is no longer needed.
- In the final phase of AUV recovery, actively steer *Frigg*'s heading to align itself to *Hugin*'s position, increasing the likelihood of a successful capture.
- Since *Hugin*'s course controller produced unwanted oscillations, investigate why this is the case.
- Instead of using the *task* reference frame to implicitly predict *Hugin*'s future lateral displacement, explore using a method of explicitly predicting where it will be at time of impact, and control that size directly. A Kalman filter may be used for this.
- Interface *Hugin*'s motion control system from HAL on *Frigg*, so that *Hugin* can aid in the final stage of the recovery process.

- Change the design of the LARS to increase tolerances for recovery, e.g., by increasing the capture width.
- Currently, there is no way of automatically detecting whether or not *Hugin* has mechanically latched onto the *Stinger*. Such a signal is required to perform the recovery process autonomously.

References

Borhaug, Even, A. Pavlov and Kristin Y. Pettersen (2008). 'Integral LOS control for path following of underactuated marine surface vessels in the presence of constant ocean currents'. In: *Proceedings of the 47th IEEE Conference on Decision and Control*. Cancun, Mexico, pp. 4984–4991. DOI: 10.1109/CDC.2008.4739352.

Breivik, Morten and Jon-Erik Loberg (2011). 'A Virtual Target-Based Underway Docking Procedure for Unmanned Surface Vehicles'. In: *Proceedings of the 18th IFAC World Congress*. Vol. 44. 1. Elsevier BV, pp. 13630–13635. DOI: 10.3182/20110828-6-it-1002.02969.

Caharija, Walter, Kristin Y. Pettersen, Marco Bibuli, Pedro Calado, Enrica Zereik, José Braga, Jan Tommy Gravdahl, Asgeir J. Sørensen, Milan Milovanović and Gabriele Bruzzone (2016). 'Integral Line-of-Sight Guidance and Control of Underactuated Marine Vehicles: Theory, Simulations, and Experiments'. In: *IEEE Transactions on Control Systems Technology* 24.5, pp. 1623–1642. DOI: 10.1109/TCST.2015.2504838.

Hagen, Per Espen, Øyvind Hegrenes, Bjørn Jalving, Øivind Midtgaard, Martin Wiig and Ove Kent Hagen (2009). 'Making AUVs Truly Autonomous'. In: *Underwater Vehicles*. Ed. by Alexander V. Inzartsev. InTech. Chap. 8, pp. 129–152. ISBN: 9789537619497.

Jalving, Bjørn, Jon Kristensen and Nils Størkersen (1998). 'Program Philosophy and Software Architecture for the HUGIN Seabed Surveying UUV'. In: *Proceedings of IFAC CAMS*. Fukuoka, Japan, pp. 211–216. DOI: 10.1016/S1474-6670(17)38442-2.

Krogstad, Thomas Røbekk, Kim Mathiassen, Else-Line Malene Ruud, Rikke Amilde Seehuus, Aleksander Skjerlie Simonsen and Martin Syre Wiig (2020). *HAL - A decisional autonomy module for unmanned systems*. FFI-report 20/00896. Norwegian Defence Research Establishment.

Larsen, Martin Vonheim (2022). *Tracktor 2*. A Flexible Tracking Framework for Autonomous Systems. FFI-report 22/01403. Norwegian Defence Research Establishment.

Rundhovde, Marius, Glenn Bitar, Fredrik Hermansen, Else-Line Malene Ruud, Jarle Sandrib and Ragnar Smestad (2022). *Unmanned Surface Vessel Autonomy for Cooperative Mine Sweeping Capabilities*. FFI-report 22/01517. Norwegian Defence Research Establishment.

Ruud, Else-Line Malene, Jarle Vandvik Selvåg, Fredrik Hermansen, Thomas Røbekk Krogstad and Jarle Sandrib (2020). *USV for future maritime mine counter measures*. FFI-report 20/00338. Norwegian Defence Research Establishment.

Sarda, Edoardo I. and Manhar R. Dhanak (2017). 'A USV-Based Automated Launch and Recovery System for AUVs'. In: *IEEE Journal of Oceanic Engineering* 42.1, pp. 37–55. DOI: 10.1109/JOE.2016.2554679.

Simonsen, Aleksander S. and Else-Line M. Ruud (2020). 'The Application of a Flexible Leader-Follower Control Algorithm to Different Mobile Autonomous Robots'. In: *Proceedings of the IEEE/RSJ International Conference on Intelligent Robots and Systems (IROS)*. Virtual, pp. 11561–11566. DOI: 10.1109/IROS45743.2020.9341780.

Szczotka, Marek (2022). 'AUV launch & recovery handling simulation on a rough sea'. In: *Ocean Engineering* 246. DOI: 10.1016/j.oceaneng.2021.110509.

Zarayskaya, Yulia, Craig Wallace, Rochelle Wigley, Karolina Zwolak, Evgenia Bazhenova, Aileen Bohan, Mohamed Elsaied, Jaya Roperez, Masanao Sumiyoshi, Seeboruth Sattiabaruth, Wetherbee Dorshow, Tomer Ketter, Hadar Sade, Alison Proctor, Ivan Ryzhov, Neil Tinmouth, Ben Simpson and Stian Michael Kristoffersen (2019). 'GEBCO-NF Alumni Team Technology Solution for Shell Ocean Discovery XPRIZE Final Round'. In: *Proceedings of OCEANS*. Marseille, France. DOI: 10.1109/OCEANSE.2019.8867201.

About FFI

The Norwegian Defence Research Establishment (FFI) was founded 11th of April 1946. It is organised as an administrative agency subordinate to the Ministry of Defence.

FFI's mission

FFI is the prime institution responsible for defence related research in Norway. Its principal mission is to carry out research and development to meet the requirements of the Armed Forces. FFI has the role of chief adviser to the political and military leadership. In particular, the institute shall focus on aspects of the development in science and technology that can influence our security policy or defence planning.

FFI's vision

FFI turns knowledge and ideas into an efficient defence.

FFI's characteristics

Creative, daring, broad-minded and responsible.

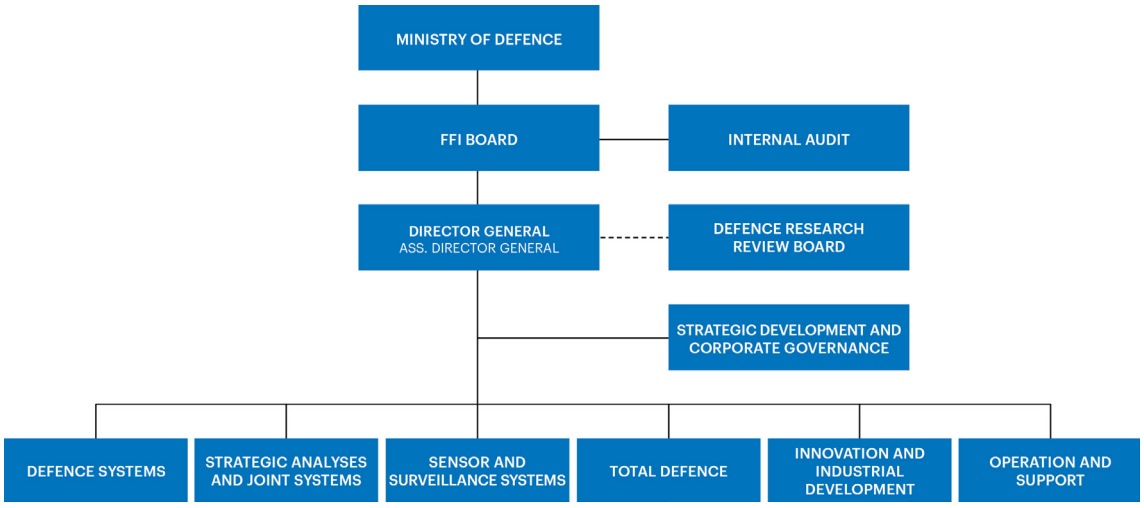

Forsvarets forskningsinstitutt (FFI)
Postboks 25
2027 Kjeller

Besøksadresse:
Kjeller: Instituttveien 20, Kjeller
Horten: Nedre vei 16, Karljohansvern, Horten

Telefon: 91 50 30 03
E-post: post@ffi.no
ffi.no

Norwegian Defence Research Establishment (FFI)
PO box 25
NO-2027 Kjeller
NORWAY

Visitor address:
Kjeller: Instituttveien 20, Kjeller
Horten: Nedre vei 16, Karljohansvern, Horten

Telephone: +47 91 50 30 03
E-mail: post@ffi.no
ffi.no/en